HAL
open science

The imprint of the extragalactic background light in the gamma-ray spectra of blazars

Markus Ackermann, M. Ajello, A. Allafort, P. Schady, Luca Baldini, Jean Ballet, Guido Barbiellini, D. Bastieri, R. Bellazzini, R. D. Blandford, et al.

To cite this version:

Markus Ackermann, M. Ajello, A. Allafort, P. Schady, Luca Baldini, et al.. The imprint of the extragalactic background light in the gamma-ray spectra of blazars. Science, 2012, 338 (6111), pp.1190-1192. 10.1126/science.1227160 . cea-00863061

HAL Id: cea-00863061

https://cea.hal.science/cea-00863061

Submitted on 21 Oct 2019

HAL is a multi-disciplinary open access archive for the deposit and dissemination of scientific research documents, whether they are published or not. The documents may come from teaching and research institutions in France or abroad, or from public or private research centers.

L'archive ouverte pluridisciplinaire **HAL**, est destinée au dépôt et à la diffusion de documents scientifiques de niveau recherche, publiés ou non, émanant des établissements d'enseignement et de recherche français ou étrangers, des laboratoires publics ou privés.

arXiv:1211.1671v1 [astro-ph.CO] 7 Nov 2012

The Imprint of The Extragalactic Background Light in the Gamma-Ray Spectra of Blazars

M. Ackermann[1], M. Ajello[2,3]†, A. Allafort[2], P. Schady[4], L. Baldini[5], J. Ballet[6], G. Barbiellini[7,8], D. Bastieri[9,10], R. Bellazzini[11], R. D. Blandford[2], E. D. Bloom[2], A. W. Borgland[2], E. Bottacini[2], A. Bouvier[12], J. Bregeon[11], M. Brigida[13,14], P. Bruel[15], R. Buehler[2]∗, S. Buson[9,10], G. A. Caliandro[16], R. A. Cameron[2], P. A. Caraveo[17], E. Cavazzuti[18], C. Cecchi[19,20], E. Charles[2], R.C.G. Chaves[6], A. Chekhtman[21], C. C. Cheung[22], J. Chiang[2], G. Chiaro[23], S. Ciprini[24,20], R. Claus[2], J. Cohen-Tanugi[25], J. Conrad[26,27,28], S. Cutini[18], F. D'Ammando[19,29,30], F. de Palma[13,14], C. D. Dermer[31], S. W. Digel[2], E. do Couto e Silva[2], A. Domínguez[12], P. S. Drell[2], A. Drlica-Wagner[2], C. Favuzzi[13,14], S. J. Fegan[15], W. B. Focke[2], A. Franckowiak[2], Y. Fukazawa[32], S. Funk[2], P. Fusco[13,14], F. Gargano[14], D. Gasparrini[18], N. Gehrels[33], S. Germani[19,20], N. Giglietto[13,14], F. Giordano[13,14], M. Giroletti[34], T. Glanzman[2], G. Godfrey[2], I. A. Grenier[6], J. E. Grove[31], S. Guiriec[33], M. Gustafsson[9], D. Hadasch[16], M. Hayashida[2,35], E. Hays[33], M. S. Jackson[36,27], T. Jogler[2], J. Kataoka[37], J. Knödlseder[38,39], M. Kuss[11], J. Lande[2], S. Larsson[26,27,40], L. Latronico[41], F. Longo[7,8], F. Loparco[13,14], M. N. Lovellette[31], P. Lubrano[19,20], M. N. Mazziotta[14], J. E. McEnery[33,42], J. Mehault[25], P. F. Michelson[2], T. Mizuno[43], C. Monte[13,14], M. E. Monzani[2], A. Morselli[44], I. V. Moskalenko[2], S. Murgia[2], A. Tramacere[45], E. Nuss[25], J. Greiner[4], M. Ohno[46], T. Ohsugi[43], N. Omodei[2], M. Orienti[34], E. Orlando[2], J. F. Ormes[47], D. Paneque[48,2], J. S. Perkins[33,49,50,51], M. Pesce-Rollins[11], F. Piron[25], G. Pivato[10], T. A. Porter[2,2], S. Rainò[13,14], R. Rando[9,10], M. Razzano[11,12], S. Razzaque[21], A. Reimer[52,2]‡, O. Reimer[52,2], L. C. Reyes[53], S. Ritz[12], A. Rau[4], C. Romoli[10], M. Roth[54], M. Sánchez-Conde[2], D.A. Sanchez[55], J. D. Scargle[56], C. Sgrò[11], E. J. Siskind[57], G. Spandre[11], P. Spinelli[13,14], Łukasz Stawarz[46,58], D. J. Suson[59], H. Takahashi[32], T. Tanaka[2], J. G. Thayer[2], D. J. Thompson[33], L. Tibaldo[9,10], M. Tinivella[11], D. F. Torres[16,60], G. Tosti[19,20], E. Troja[33,61], T. L. Usher[2], J. Vandenbroucke[2], V. Vasileiou[25], G. Vianello[2,62], V. Vitale[44,63], A. P. Waite[2], B. L. Winer[64], K. S. Wood[31], M. Wood[2]

1. Deutsches Elektronen Synchrotron DESY, D-15738 Zeuthen, Germany

2. W. W. Hansen Experimental Physics Laboratory, Kavli Institute for Particle Astrophysics and Cosmology, Department of Physics and SLAC National Accelerator Laboratory, Stanford University, Stanford, CA 94305, USA

3. Space Sciences Laboratory, 7 Gauss Way, University of California, Berkeley, CA 94720-7450, USA

4. Max-Planck Institut für extraterrestrische Physik, 85748 Garching, Germany

5. Università di Pisa and Istituto Nazionale di Fisica Nucleare, Sezione di Pisa I-56127 Pisa, Italy

6. Laboratoire AIM, CEA-IRFU/CNRS/Université Paris Diderot, Service d'Astrophysique, CEA Saclay, 91191 Gif sur Yvette, France

7. Istituto Nazionale di Fisica Nucleare, Sezione di Trieste, I-34127 Trieste, Italy

8. Dipartimento di Fisica, Università di Trieste, I-34127 Trieste, Italy

9. Istituto Nazionale di Fisica Nucleare, Sezione di Padova, I-35131 Padova, Italy

10. Dipartimento di Fisica e Astronomia "G. Galilei", Università di Padova, I-35131 Padova, Italy

11. Istituto Nazionale di Fisica Nucleare, Sezione di Pisa, I-56127 Pisa, Italy

12. Santa Cruz Institute for Particle Physics, Department of Physics and Department of Astronomy and Astrophysics, University of California at Santa Cruz, Santa Cruz, CA 95064, USA

13. Dipartimento di Fisica "M. Merlin" dell'Università e del Politecnico di Bari, I-70126 Bari, Italy

14. Istituto Nazionale di Fisica Nucleare, Sezione di Bari, 70126 Bari, Italy

15. Laboratoire Leprince-Ringuet, École polytechnique, CNRS/IN2P3, Palaiseau, France

16. Institut de Ciències de l'Espai (IEEE-CSIC), Campus UAB, 08193 Barcelona, Spain

17. INAF-Istituto di Astrofisica Spaziale e Fisica Cosmica, I-20133 Milano, Italy

18. Agenzia Spaziale Italiana (ASI) Science Data Center, I-00044 Frascati (Roma), Italy

19. Istituto Nazionale di Fisica Nucleare, Sezione di Perugia, I-06123 Perugia, Italy

20. Dipartimento di Fisica, Università degli Studi di Perugia, I-06123 Perugia, Italy

21. Center for Earth Observing and Space Research, College of Science, George Mason University, Fairfax, VA 22030, resident at Naval Research Laboratory, Washington, DC 20375, USA

22. National Research Council Research Associate, National Academy of Sciences, Washington, DC 20001, resident at Naval Research Laboratory, Washington, DC 20375, USA

23. INFN and Dipartimento di Fisica e Astronomia ”G. Galilei”, Università di Padova, I-35131 Padova, Italy,

24. ASI Science Data Center, I-00044 Frascati (Roma), Italy

25. Laboratoire Univers et Particules de Montpellier, Université Montpellier 2, CNRS/IN2P3, Montpellier, France

26. Department of Physics, Stockholm University, AlbaNova, SE-106 91 Stockholm, Sweden

27. The Oskar Klein Centre for Cosmoparticle Physics, AlbaNova, SE-106 91 Stockholm, Sweden

28. Royal Swedish Academy of Sciences Research Fellow, funded by a grant from the K. A. Wallenberg Foundation

29. IASF Palermo, 90146 Palermo, Italy

30. INAF-Istituto di Astrofisica Spaziale e Fisica Cosmica, I-00133 Roma, Italy

31. Space Science Division, Naval Research Laboratory, Washington, DC 20375-5352, USA

32. Department of Physical Sciences, Hiroshima University, Higashi-Hiroshima, Hiroshima 739-8526, Japan

33. NASA Goddard Space Flight Center, Greenbelt, MD 20771, USA

34. INAF Istituto di Radioastronomia, 40129 Bologna, Italy

35. Department of Astronomy, Graduate School of Science, Kyoto University, Sakyo-ku, Kyoto 606-8502, Japan

36. Department of Physics, Royal Institute of Technology (KTH), AlbaNova, SE-106 91 Stockholm, Sweden

37. Research Institute for Science and Engineering, Waseda University, 3-4-1, Okubo, Shinjuku, Tokyo 169-8555, Japan

38. CNRS, IRAP, F-31028 Toulouse cedex 4, France

39. GAHEC, Université de Toulouse, UPS-OMP, IRAP, Toulouse, France

40. Department of Astronomy, Stockholm University, SE-106 91 Stockholm, Sweden

41. Istituto Nazionale di Fisica Nucleare, Sezione di Torino, I-10125 Torino, Italy

42. Department of Physics and Department of Astronomy, University of Maryland, College Park, MD 20742, USA

43. Hiroshima Astrophysical Science Center, Hiroshima University, Higashi-Hiroshima, Hiroshima 739-8526, Japan

44. Istituto Nazionale di Fisica Nucleare, Sezione di Roma “Tor Vergata”, I-00133 Roma, Italy

45. INTEGRAL Science Data Centre, CH-1290 Versoix, Switzerland

46. Institute of Space and Astronautical Science, JAXA, 3-1-1 Yoshinodai, Chuo-ku, Sagamihara, Kanagawa 252-5210, Japan

47. Department of Physics and Astronomy, University of Denver, Denver, CO 80208, USA

48. Max-Planck-Institut für Physik, D-80805 München, Germany

49. Department of Physics and Center for Space Sciences and Technology, University of Maryland Baltimore County, Baltimore, MD 21250, USA

50. Center for Research and Exploration in Space Science and Technology (CRESST) and NASA Goddard Space Flight Center, Greenbelt, MD 20771, USA

51. Harvard-Smithsonian Center for Astrophysics, Cambridge, MA 02138, USA

52. Institut für Astro- und Teilchenphysik and Institut für Theoretische Physik, Leopold-Franzens-Universität Innsbruck, A-6020 Innsbruck, Austria

53. Department of Physics, California Polytechnic State University, San Luis Obispo, CA 93401, USA

54. Department of Physics, University of Washington, Seattle, WA 98195-1560, USA

55. Max-Planck-Institut für Kernphysik, D-69029 Heidelberg, Germany

56. Space Sciences Division, NASA Ames Research Center, Moffett Field, CA 94035-1000, USA

57. NYCB Real-Time Computing Inc., Lattingtown, NY 11560-1025, USA

58. Astronomical Observatory, Jagiellonian University, 30-244 Kraków, Poland

59. Department of Chemistry and Physics, Purdue University Calumet, Hammond, IN 46323-2094, USA

60. Institució Catalana de Recerca i Estudis Avançats (ICREA), Barcelona, Spain

61. NASA Postdoctoral Program Fellow, USA

62. Consorzio Interuniversitario per la Fisica Spaziale (CIFS), I-10133 Torino, Italy

63. Dipartimento di Fisica, Università di Roma "Tor Vergata", I-00133 Roma, Italy

64. Department of Physics, Center for Cosmology and Astro-Particle Physics, The Ohio State University, Columbus, OH 43210, USA

† majello@slac.stanford.edu, *buehler@stanford.edu, ‡ anita.reimer@uibk.ac.at

The light emitted by stars and accreting compact objects through the history of the Universe is encoded in the intensity of the extragalactic background light (EBL). Knowledge of the EBL is important to understand the nature of star formation and galaxy evolution, but direct measurements of the EBL are limited by Galactic and other foreground emissions. Here we report an absorption feature seen in the combined spectra of a sample of gamma-ray blazars out to a redshift of z∼1.6. This feature is caused by attenuation of gamma rays by the EBL at optical to UV frequencies, and allowed us to measure the EBL flux density in this frequency band.

The bulk of the intergalactic gas in the Universe must have been reionized between the epoch of cosmic recombination, when the Universe was only 300,000 years old (z∼1100), and 1 billion years later (z∼6) as indicated observationally by the spectra of distant quasi-stellar objects (*1*). However, the sources, modes and nature of this cosmic reionization are largely unknown because most of this redshift range has yet to be explored. Photoionization by UV radiation, produced by the first stars and galaxies of the Universe, represents the primary suspect for the ionizing process (*2,3*). Direct detection of the UV radiation fields is thus of fundamental importance, but at present extremely difficult (*3*).

An indirect but powerful means of probing the diffuse radiation fields is through γ-γ absorption of high-energy gamma rays (*4–6*). In this process, a gamma-ray photon of energy E_γ and an EBL photon of energy E_{EBL} annihilate and create an electron-positron pair. This process occurs for head-on collisions when (e.g.) $E_\gamma \times E_{EBL} \geq 2(m_e c^2)^2$, where $m_e c^2$ is the rest mass energy of the electron. This introduces an attenuation in the spectra of gamma-ray sources above a critical gamma-ray energy of $E_{crit}(z) \approx 170(1+z)^{-2.38}$ GeV (*7,8*).

The detection of the gamma-ray horizon (i.e. the point beyond which the emission of gamma-ray sources is strongly attenuated) is one of the primary scientific drivers of the *Fermi* Gamma-ray Space Telescope (*9–11*). Several attempts have been made in the past but none detected the long-sought EBL attenuation (*12–14*). So far, limits on the EBL density have been inferred from the absence of absorption features in the spectra of individual blazars (*13, 15*), distant galaxies with bright gamma-ray emission powered by matter accreting onto central, massive black holes. While this feature is indeed difficult to constrain for a single source, we show that it is detected collectively in the gamma-ray spectra of a sample of blazars as a cut-off that changes amplitude and energy with redshift. We searched for an attenuation of the spectra

of blazars in the 1–500 GeV band using the first 46 months of observations of the Large Area Telescope (LAT) on board the *Fermi* satellite. At these energies gamma rays are absorbed by EBL photons in the optical to UV range. Thanks to the large energy and redshift coverage, *Fermi*-LAT measures the intrinsic (i.e. unabsorbed) spectrum up to $\sim$100 GeV for any blazar at z$<$0.2, and up to $\sim$15 GeV for any redshift.

The LAT has detected $>$1000 blazars to date (*16*). We restricted our search to a subset of 150 blazars of the BL Lacertae (BL Lac) type that are significantly detected above 3 GeV, because of the expected lack of intrinsic absorption (*17*). The sample covers a redshift range 0.03–1.6 (*18, 19*). The critical energy is therefore always $\geq$25 GeV, which means that the spectrum measured below this energy is unabsorbed and a true representation of the intrinsic spectrum of the source. We thus determined the intrinsic source spectrum relying on data between 1 GeV and the critical energy E_{crit} and extrapolated it to higher energies. By combining all the spectra we were able to determine, the average deviation, above the critical energy, of the measured spectra from the intrinsic ones, which ultimately provides a measurement of the optical depth $\tau_{\gamma\gamma}$.

The analysis was performed using the *Fermi* Science Tools (*20*). We determined the spectral parameters of each blazar by maximizing the likelihood of a given source model. The model comprised the Galactic and isotropic diffuse components and all sources in the second *Fermi* LAT catalog (*21*) within a region of interest (ROI) of 15° radius. We modeled the spectra of the sources in our sample as parabolic in the logarithmic space of energy and flux (see Eq. 2 in (*21*) for a definition). Their spectra were modified by a term $e^{-\tau_{\gamma\gamma}(E,z)}$ that describes the absorption of gamma-ray photons on the EBL. In the above we defined $\tau_{\gamma\gamma}(E,z) = b \cdot \tau_{\gamma\gamma}^{model}(E,z)$, where the $\tau_{\gamma\gamma}^{model}(E,z)$ is the optical depth predicted by EBL models (*7, 22–25*) and b is a scaling variable, left free in the likelihood maximization. In particular, this allowed us to assess the likelihood of two important scenarios: i) there is no EBL attenuation (b=0), ii) the model prediction is correct (b=1).

We combined the data from all the ROIs in a global fit that determined the common parameter b for a given EBL model (see Table S1). All those models with a minimal EBL density based on (or compatible with) resolved galaxy counts (*2, 7, 24–27*) were found to be acceptable descriptions of the *Fermi* data (i.e are consistent with b=1 within $\approx$25 %, see also Figure 1) yielding a significance of the absorption feature of up to $\sim 6\,\sigma$. Models that predict a larger intensity of the EBL particularly in the UV (*22, 23*) would produce a stronger-than-observed attenuation feature and are therefore incompatible with the *Fermi* observations. Our measurement points to a minimal level of the optical-UV EBL up to redshift z$\approx$1.6 which combined with the upper limits (*15, 28, 29*) derived at lower redshift (using observations of blazars at TeV energies) on the near-infrared EBL highlights the conclusion that most of the EBL intensity can be explained by the measured galaxy emission.

Our measurement relies on the accuracy of the extrapolation of the intrinsic spectra of the sources above the critical energy (*30*). This in turn depends on a precise description of the gamma-ray spectra by our source parametrization. To verify that this is the case and to exclude the possibility that the detected absorption feature is intrinsic to the gamma-ray sources (*17*), we

performed the analysis in 3 independent redshift intervals (z<0.2, 0.2≤z<0.5, and 0.5≤z<1.6). The deviations from the intrinsic spectra in the three redshift intervals are displayed in Figure 2. In the local Universe (z<0.2), EBL absorption is negligible in most of the *Fermi*-LAT energy band (E_{crit} ≥120 GeV). The lowest redshift interval therefore reveals directly the intrinsic spectra of the sources and shows that our spectral parametrization is accurate (*18*). The absorption feature is clearly visible above the critical energy in the higher redshift bins. Its amplitude and modulation in energy evolve with redshift as expected for EBL absorption. In principle, the observed attenuation could be due to a spectral cut-off that is intrinsic to the gamma-ray sources. The absence of a cut-off in the spectra of sources with z<0.2 would require that the properties of BL Lacs change with redshift or luminosity. It remains an issue of debate whether such evolution exists (*31–34*). However, in case it were present, the intrinsic cut-off would be expected to evolve differently with redshift than we observe. To illustrate this effect, we fitted the blazar sample assuming that all the sources have an exponential cut-off at an energy E_0. From source to source the observed cut-off energy changes because of the source redshift and because we assumed that blazars as a population are distributed in a sequence such as that proposed in (*31–34*). E_0 was fitted to the data globally like b above. As apparent from Figure 2, it appears difficult to reconcile the observed feature with an intrinsic characteristic of the blazars' spectra. We therefore associate the spectral feature to the EBL absorption.

At energies ≤100 GeV, gamma rays observed at Earth and coming from redshift ≥1 interact mostly with UV photons of ≥5 electron volts. An UV background in excess of the light emitted by resolved galaxies can be produced locally by AGN or at higher redshift (z≈7-15) by low-metallicity massive stars (*35*). By comparing the results from the best-fit EBL models, we measured the UV component of the EBL to have an intensity of 3(±1) nW m^{-2} sr^{-1} at z≈1. A contribution to the UV background from AGN as large as the one predicted by (*36*) (i.e., ≈ 10 nW m^{-2} sr^{-1}) and used in the EBL model of (*22*) is thus excluded by our analysis at high confidence. However, the recent prediction (*37*) of the UV background from AGN ($\approx$ 2 nW m^{-2} sr^{-1}) is in agreement with the *Fermi* measurement. Direct measurements of the extragalactic UV background are hampered by the strong dust-scattered Galactic radiation (*38*). The agreement between the intensity of the UV background as measured with *Fermi* and that due to galaxies individually resolved by the Hubble Space Telescope (*39*) (3±1 nW m^{-2} sr^{-1} versus 2.9–3.9 nW m^{-2} sr^{-1}, respectively) shows that the room for any residual diffuse UV emission is small. This conclusion is reinforced by the good agreement of the *Fermi* measurement and the estimate of the average UV background, at z≥1.7, of 2.2–4.0 nW m^{-2} sr^{-1} using the proximity effect in quasar spectra (*40*).

Zero-metallicity population-III stars or low-metallicity population-II stars are thought to be the first stars to form in the Universe and formally marked the end of the dark ages when, with their UV light, these objects started ionizing the intergalactic medium (*41*). These stars, whose mass might have exceeded one hundred times the mass of our Sun, are also believed to be responsible for creating the first metals and dispersing them in the intergalactic medium (*42–44*). A very large contribution of population-III stars to the near-infrared EBL had already been excluded by (*15*). Our measurement constrains, according to (*45,46*), the redshift of maximum

formation of low-metallicity stars to be at z≥10 and its peak co-moving star-formation rate to be lower than 0.5 $M_\odot$ Mpc^{-3} yr^{-1}. This upper limit is already of the same order of the peak star-formation rate of 0.2–0.6 $M_\odot$ Mpc^{-3} yr^{-1} proposed by (*47*) and suggests that the peak star-formation rate might be much lower as proposed by (*48*).

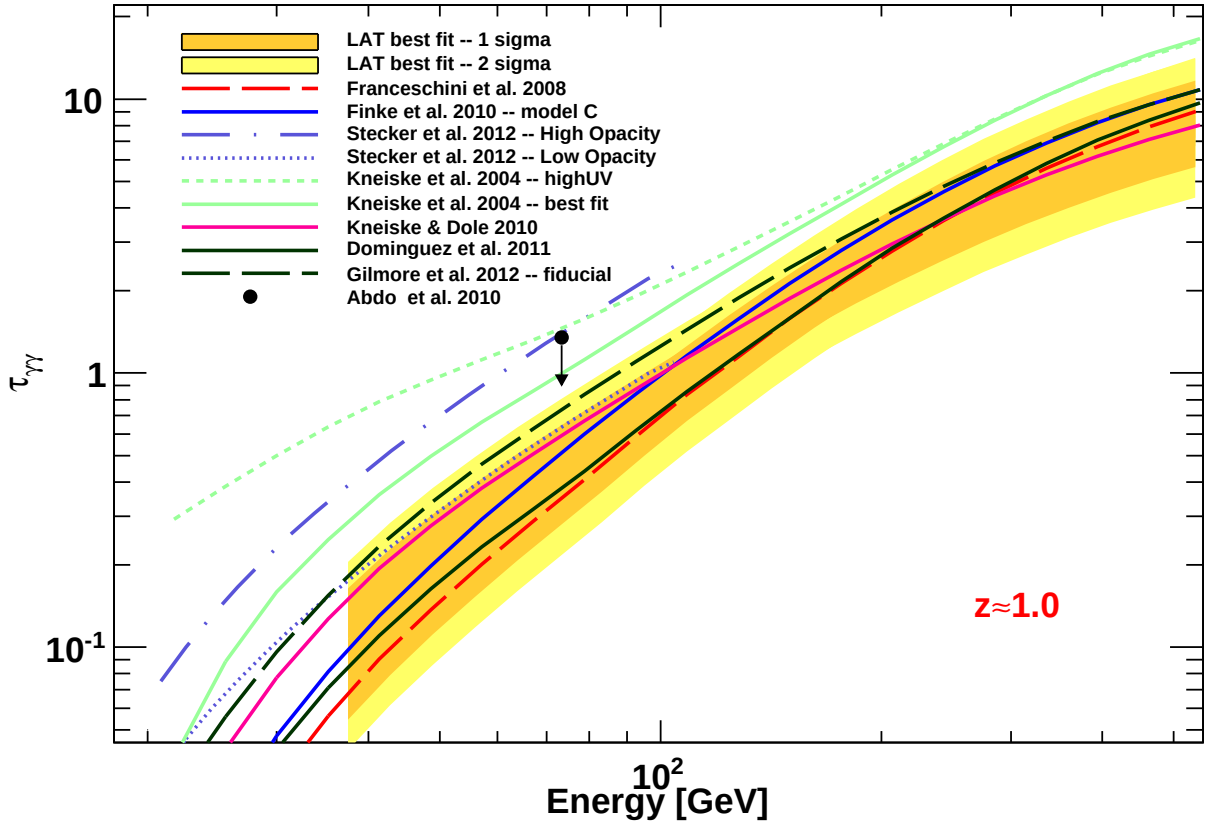

Figure 1 Measurement, at the 68 % and 95 % confidence levels (including systematic uncertainties added in quadrature), of the opacity $\tau_{\gamma\gamma}$ from the best fits to the *Fermi* data compared to predictions of EBL models. The plot shows the measurement at z≈1 which is the average redshift of the most constraining redshift interval (i.e. 0.5≤z<1.6). The *Fermi*-LAT measurement was derived combining the limits on the best-fit EBL models. The downward arrow represents the 95 % upper limit on the opacity at z=1.05 derived in (*13*). For clarity this figure shows only a selection of the models we tested while the full list is reported in Table S1. The EBL models of (*49*), which are not defined for E≥$250/(1+z)$ GeV and thus could not be used, are reported here for completeness.

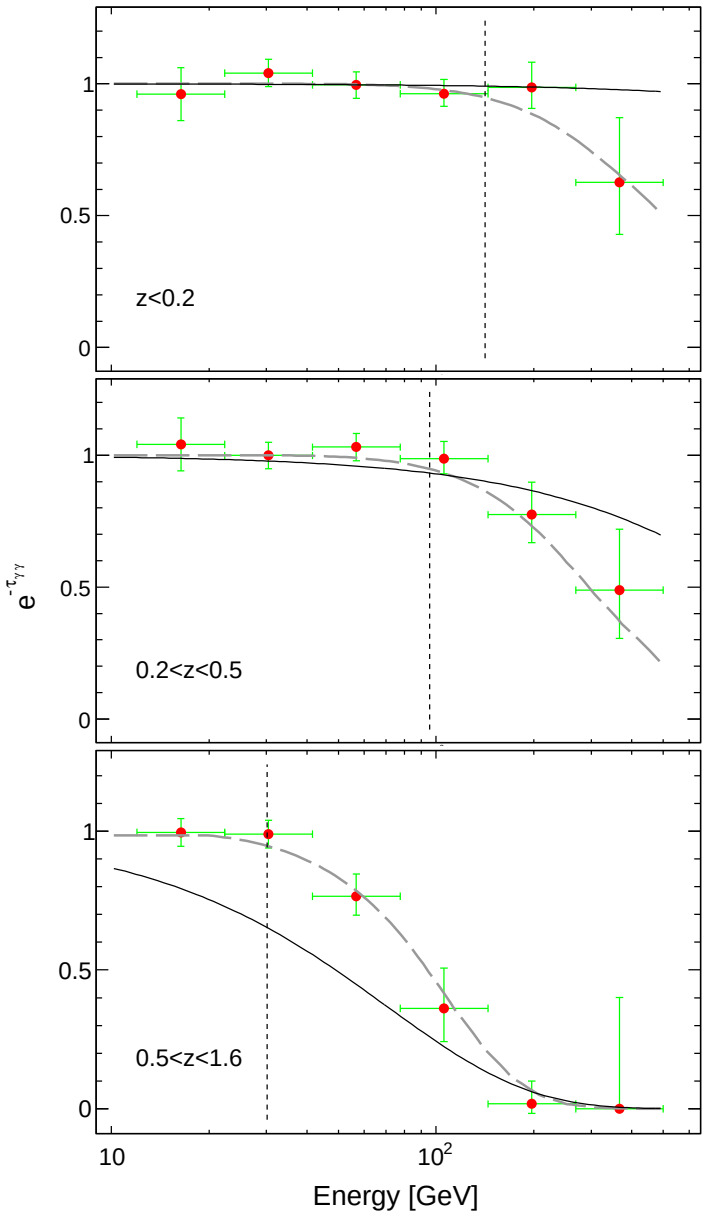

Figure 2 Absorption feature present in the spectra of BL Lacertae objects as a function of increasing redshift (data points, from top to bottom). The dashed curves show the attenuation expected for the sample of sources by averaging, in each redshift and energy bin, the opacities of the sample (the model of (*7*) was used) and multiplying this average by the best-fit scaling parameter b obtained independently in each redshift interval. The vertical line shows the critical energy E_{crit} below which $\leq 5\,\%$ of the source photons are absorbed by the EBL. The thin solid curve represents the best-fit model assuming that all the sources have an intrinsic exponential cut-off and that blazars follow the blazar sequence model of (*32,33*).

References and Notes

1. X. Fan, *et al.*, *Astronomical Journal* **132**, 117 (2006).
2. R. C. Gilmore, P. Madau, J. R. Primack, R. S. Somerville, F. Haardt, *Monthly Notices of the Royal Astronomical Society* **399**, 1694 (2009).
3. S. Inoue, *et al.*, *Monthly Notices of the Royal Astronomical Society* **404**, 1938 (2010).
4. R. J. Gould, G. Schréder, *Physical Review Letters* **16**, 252 (1966).
5. G. G. Fazio, F. W. Stecker, *Nature* **226**, 135 (1970).
6. F. W. Stecker, O. C. de Jager, M. H. Salamon, *The Astrophysical Journall* **390**, L49 (1992).
7. A. Franceschini, G. Rodighiero, M. Vaccari, *Astronomy and Astrophysics* **487**, 837 (2008).
8. We define the critical energy E_{crit} such that less than 5 % of the source photons are absorbed for the EBL model of (*7*) below this energy.
9. D. H. Hartmann, *The First GLAST Symposium*, S. Ritz, P. Michelson, C. A. Meegan, eds. (2007), vol. 921 of *American Institute of Physics Conference Series*, pp. 24–25.
10. F. W. Stecker, *The First GLAST Symposium*, S. Ritz, P. Michelson, C. A. Meegan, eds. (2007), vol. 921 of *American Institute of Physics Conference Series*, pp. 237–239.
11. A. Kashlinsky, D. Band, *The First GLAST Symposium*, S. Ritz, P. Michelson, C. A. Meegan, eds. (2007), vol. 921 of *American Institute of Physics Conference Series*, pp. 243–245.
12. K. Mannheim, S. Westerhoff, H. Meyer, H. H. Fink, *The Astrophysical Journal* **315**, 77 (1996).
13. A. A. Abdo, *et al.*, *The Astrophysical Journal* **723**, 1082 (2010).
14. M. Raue, *Astronomy and Astrophysics* **520**, A34 (2010).
15. F. Aharonian, *et al.*, *Nature* **440**, 1018 (2006).
16. M. Ackermann, *et al.*, *The Astrophysical Journal* **743**, 171 (2011).
17. A. Reimer, *The Astrophysical Journal* **665**, 1023 (2007).
18. A more detailed description is given in the supplemental online material.
19. A. Rau, *et al.*, *Astronomy and Astrophysics* **538**, A26 (2012).
20. The software to perform analysis of *Fermi* data is available at http://fermi.gsfc.nasa.gov/ssc/data/analysis/software/.

21. P. Nolan, *et al.*, *arXiv:1108.1435* (2011).

22. T. M. Kneiske, T. Bretz, K. Mannheim, D. H. Hartmann, *Astronomy and Astrophysics* **413**, 807 (2004).

23. F. W. Stecker, M. A. Malkan, S. T. Scully, *The Astrophysical Journal* **648**, 774 (2006).

24. J. D. Finke, S. Razzaque, C. D. Dermer, *The Astrophysical Journal* **712**, 238 (2010).

25. A. Domínguez, *et al.*, *Monthly Notices of the Royal Astronomical Society* **410**, 2556 (2011).

26. T. M. Kneiske, H. Dole, *Astronomy and Astrophysics* **515**, A19 (2010).

27. R. C. Gilmore, R. S. Somerville, J. R. Primack, A. Domínguez, *Monthly Notices of the Royal Astronomical Society* **422**, 3189 (2012).

28. D. Mazin, M. Raue, *Astronomy and Astrophysics* **471**, 439 (2007).

29. The MAGIC Collaboration, *et al.*, *Science* **320**, 1752 (2008).

30. We show in the supplemental material that our result is robust against conservative choices the critical energy.

31. G. Ghisellini, A. Celotti, G. Fossati, L. Maraschi, A. Comastri, *Monthly Notices of the Royal Astronomical Society* **301**, 451 (1998).

32. G. Fossati, L. Maraschi, A. Celotti, A. Comastri, G. Ghisellini, *Monthly Notices of the Royal Astronomical Society* **299**, 433 (1998).

33. G. Ghisellini, L. Maraschi, F. Tavecchio, *Monthly Notices of the Royal Astronomical Society* **396**, L105 (2009).

34. E. T. Meyer, G. Fossati, M. Georganopoulos, M. L. Lister, *The Astrophysical Journal* **740**, 98 (2011).

35. M. R. Santos, V. Bromm, M. Kamionkowski, *Monthly Notices of the Royal Astronomical Society* **336**, 1082 (2002).

36. F. Haardt, P. Madau, *The Astrophysical Journal* **461**, 20 (1996).

37. F. Haardt, P. Madau, *The Astrophysical Journal* **746**, 125 (2012).

38. S. Bowyer, *Annual Review of Astronomy and Astrophysics* **29**, 59 (1991).

39. J. P. Gardner, T. M. Brown, H. C. Ferguson, *The Astrophysical Journal* **542**, L79 (2000).

40. J. Scott, J. Bechtold, A. Dobrzycki, V. P. Kulkarni, *The Astrophysical Journal* **130**, 67 (2000).

41. V. Bromm, R. B. Larson, *Annual Review of Astronomy and Astrophysics* **42**, 79 (2004).

42. J. P. Ostriker, N. Y. Gnedin, *The Astrophysical Journal* **472**, L63 (1996).

43. T. H. Greif, J. L. Johnson, V. Bromm, R. S. Klessen, *The Astrophysical Journal* **670**, 1 (2007).

44. J. H. Wise, T. Abel, *The Astrophysical Journal* **685**, 40 (2008).

45. M. Raue, T. Kneiske, D. Mazin, *Astronomy and Astrophysics* **498**, 25 (2009).

46. R. C. Gilmore, *eprint arXiv:1109.0592* (2011).

47. V. Bromm, A. Loeb, *The Astrophysical Journal* **575**, 111 (2002).

48. L. Tornatore, A. Ferrara, R. Schneider, *Monthly Notices of the Royal Astronomical Society* **382**, 945 (2007).

49. F. W. Stecker, M. A. Malkan, S. T. Scully, *arXiv:1205.5168* (2012).

50. J. T. Stocke, *et al.*, *The Astrophysical Journals* **76**, 813 (1991).

51. C. M. Urry, P. Padovani, *Publications of the Astronomical Society of the Pacific* **107**, 803 (1995).

52. M. J. M. Marcha, I. W. A. Browne, C. D. Impey, P. S. Smith, *Monthly Notices of the Royal Astronomical Society* **281**, 425 (1996).

53. A. A. Abdo, *et al.*, *The Astrophysical Journal* **736**, 131 (2011).

54. A. A. Abdo, *et al.*, *The Astrophysical Journal* **727**, 129 (2011).

55. E. Aliu, *et al.*, *The Astrophysical Journal* **750**, 94 (2012).

56. J. R. Primack, J. S. Bullock, R. S. Somerville, *High Energy Gamma-Ray Astronomy*, F. A. Aharonian, H. J. Völk, & D. Horns, ed. (2005), vol. 745 of *American Institute of Physics Conference Series*, pp. 23–33.

57. A. Tramacere, E. Massaro, A. M. Taylor, *The Astrophysical Journal* **739**, 66 (2011).

58. E. Massaro, A. Tramacere, M. Perri, P. Giommi, G. Tosti, *Astronomy and Astrophysics* **448**, 861 (2006).

59. Fermi-LAT Collaboration, *arXiv:1206.1896* (2012).

60. R. Plaga, *Nature* **374**, 430 (1995).

61. F. Tavecchio, G. Ghisellini, G. Bonnoli, L. Foschini, *Monthly Notices of the Royal Astronomical Society* **414**, 3566 (2011).

62. A. Neronov, D. Semikoz, M. Kachelriess, S. Ostapchenko, A. Elyiv, *The Astrophysical Journall* **719**, L130 (2010).

63. I. Vovk, A. M. Taylor, D. Semikoz, A. Neronov, *The Astrophysical Journal* **747**, L14 (2012).

64. C. D. Dermer, *et al.*, *The Astrophysical Journal* **733**, L21 (2011).

65. F. Tavecchio, G. Ghisellini, G. Ghirlanda, L. Foschini, L. Maraschi, *Monthly Notices of the Royal Astronomical Society* **401**, 1570 (2010).

66. K. Mannheim, *The Astrophysical Journal* **269**, 67 (1993).

67. E. Waxman, P. Coppi, *The Astrophysical Journal* **464**, L75 (1996).

68. W. Essey, A. Kusenko, *Astroparticle Physics* **33**, 81 (2010).

Marco Ajello acknowledges generous support from the Fermi guest investigator program (proposals ID 31117 and 51258) and the Swift and the GROND teams for observing ∼hundred Fermi blazars in an effort to constrain their redshifts. The *Fermi* LAT Collaboration acknowledges generous ongoing support from a number of agencies and institutes that have supported both the development and the operation of the LAT as well as scientific data analysis. These include the National Aeronautics and Space Administration and the Department of Energy in the United States, the Commissariat à l'Energie Atomique and the Centre National de la Recherche Scientifique / Institut National de Physique Nucléaire et de Physique des Particules in France, the Agenzia Spaziale Italiana and the Istituto Nazionale di Fisica Nucleare in Italy, the Ministry of Education, Culture, Sports, Science and Technology (MEXT), High Energy Accelerator Research Organization (KEK) and Japan Aerospace Exploration Agency (JAXA) in Japan, and the K. A. Wallenberg Foundation, the Swedish Research Council and the Swedish National Space Board in Sweden. Additional support for science analysis during the operations phase is gratefully acknowledged from the Istituto Nazionale di Astrofisica in Italy and the Centre National d'Études Spatiales in France.

Supplements

Source Selection

The second LAT AGN Catalog (*16*) contains many flat-spectrum radio quasars (FSRQs) and BL Lacertae (BL Lac) objects whose spectra extend significantly above 10 GeV. The classification relies on the conventional definition of BL Lac objects outlined in (*50–52*) in which the equivalent width of the strongest optical emission line is <5 Å and the optical spectrum shows a Ca II H/K break ratio C$<$0.4. Sources are then classified also according to the position of the peak of the synchrotron component as low-synchrotron-peaked (LSP, $\nu_{peak}<10^{14}$ Hz), intermediate-synchrotron-peaked (ISP, $10^{14}<\nu_{peak}<10^{15}$ Hz), and high-synchrotron-peaked (HSP, $\nu_{peak}>10^{15}$ Hz).

FSRQs generally have soft spectra (photon index greater than 2.3) at GeV energies, making it more difficult to detect absorption features at energies greater than 10 GeV. Additionally their spectra might suffer from intrinsic absorption of gamma rays by the photons of the broad line region or of the accretion disk (*17*). This makes them non-ideal candidates to constrain the EBL. We therefore focused on the BL Lac objects. For computational reasons, only 50 sources can be analyzed in one combined likelihood fit. In order to perform our analysis in three redshift intervals we selected the 150 BL Lacs that show the largest detection significance in the 3–10 GeV energy band (the significance is always larger than 3.5 σ) with no selection on spectral shape. Most of the sources (100 out of 150) were detected with a significance $\geq 3\,\sigma$ above 10 GeV already after two years of observations (*21*). In the second LAT AGN Catalog catalog (*16*) only $\sim$190 BL Lac have a redshift measurement, so our sample is a representative set of *Fermi*-detected BL Lacs. Figure S1 shows the redshift distribution of the BL Lac objects employed in this analysis.

Data Analysis

Each source in our sample is analyzed using 46 months[1] of *Fermi* observations using version v9r27 of the Science Tools[2]. The data were filtered, removing time periods in which the instrument was not in sky-survey mode, and removing photons whose zenith angle is larger than 100° to limit contamination from the Earth limb emission. We consider only photons collected within 15° of the source position with $1\leq$E$\leq$ 500 GeV. We employ the P7SOURCE_V6[3] instrumental response function (IRF) and perform a binned likelihood analysis. The Galactic and isotropic diffuse emissions are modeled using respectively the gal_2yearp7v6_v0.fits and iso_p7v6source.txt templates.

We rely on the *Composite Likelihood* tool of the *Fermi* software to perform the likelihood maximization. This allows us to fit simultaneously the data from different ROIs with the aim of constraining the scaling parameter b that is applied to the opacity curves predicted by each

[1] From August 4th 2008 to June 1st 2012

[2] http://fermi.gsfc.nasa.gov/ssc/data/analysis/software/

[3] Our analysis is robust against change of the dataset and IRF.

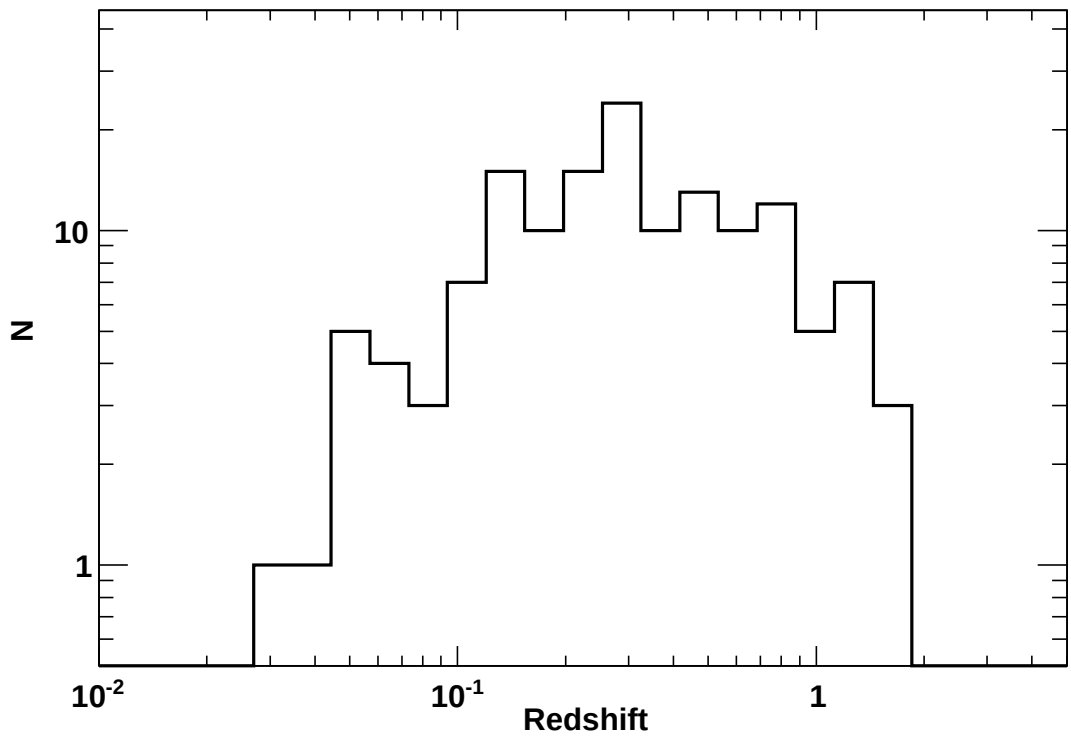

Figure S1 Redshift distribution of the BL Lac objects used in this analysis.

one of the EBL models we tested. The total number of free parameters across all ROIs in one redshift bin is approximately 1000. It is computationally unfeasible to fit all of these parameters simultaneously. We therefore proceeded in three steps. First we fit each ROI individually. The fit is performed on the entire energy band (1–500 GeV). The parameters (i.e. flux and photon index) of all the sources within 4° of the target source, along with the parameters of the diffuse components, are left free to vary. More distant sources have parameters frozen at the values measured in the second *Fermi* LAT catalog (*21*), unless the inspection of the residual map showed that a given source underwent strong variability. In that case, the normalizations of those sources were left free in the fit. The spectra of the sources of interest are modeled using a *LogParabola* model (*21*). We then proceed to re-optimize the parameters of the source of interest in each ROI up to that energy for which the EBL absorption becomes no longer negligible (see the definition of E_{crit} in the main text). In the third step we fix the curvature of the *LogParabola* model to the value obtained in the previous fit. Finally, we use the *Composite Likelihood* to constrain the gamma-ray opacity. The *Composite Likelihood* allows the user to tie any parameters between any ROIs. In our case the only tied parameter is the renormalization

factor b of the opacity of a given EBL model.

The significance of our finding can be evaluated using the Test Statistic (TS) as $TS = 2(log\mathscr{L}(b) - log\mathscr{L}(b=0))$, where $\mathscr{L}$ is the likelihood function and the $b = 0$ case (i.e. no EBL absorption) represents the null hypothesis. Since the null hypothesis is a special case of the hypothesis we test, we expect the TS to be distributed as a χ^2 with one degree of freedom (see also next sections). This allows one to transform the TS into the corresponding number of standard deviations of a Gaussian distribution as $n_\sigma = \sqrt{TS}$.

Modeling the Intrinsic Blazar Spectrum

One of the basic assumptions of this analysis is that on average the spectrum of a BL Lac blazar can be adequately modeled using a *LogParabola* in the 1-500 GeV band. Figure S2 shows the residuals of the best fits to all the sources in the z<0.2 interval. It is apparent that the *LogParabola* provides a good representation of the spectra of blazars in our sample.

In an additional test we artificially decreased the critical energy E_{crit} for all the sources in the z<0.2 interval from the typical ≥120 GeV (for z<0.2) to ∼40 GeV which is representative of the z≥0.5 case. Even in this case the results are unchanged, showing that the properties of the intrinsic spectrum can be determined over a more restricted energy range and can be safely extrapolated above the critical energy.

Blazars are however known to have complex spectra that cannot always be modeled using simple empirical functions. To further test our basic assumption, we fit the spectra of bright blazars with coverage in the GeV and TeV band. We rely on the published spectra of Mrk 421 (*53*), Mrk 501 (*54*) and RBS 0413 (*55*). We find that in the energy range relevant for the present analysis the *LogParabola* model provides an adequate fit to all these spectra. A further confirmation comes from our validation studies using simulations of broad-band blazar spectra (see next sections). We thus conclude that in a small energy range like the one adopted here (1–500 GeV), the *LogParabola* is an adequate representation of the intrinsic blazar spectrum.

Results

Table S1 reports the results of the joint-likelihood fit for all the predictions of the EBL models we tested. In many cases, a given EBL model (because of tunable parameters or uncertainties connected to e.g, galaxy evolution, star-formation rate etc.) comprises several different predictions for the opacity. In this case, we use these prediction at face value and test them against our observations. All the models with the exclusion of (*22*)[4] rely on a standard concordance cosmology (H_0=70 km s^{-1} Mpc^{-1}, Ω_M=1-Ω_Λ=0.3). For each model we report the significance of the absorption feature detected once we allow the opacity to be renormalized by b. The significances have been obtained as a square root of the sum of the TS in the 3 redshift intervals while

[4]The model of (*22*) adopts a value of H_0=65 km s^{-1} Mpc^{-1}. We checked that neglecting the change of H_0 for the model of (*22*) introduces an error on the opacity of <7 % which has negligible influence on our analysis..

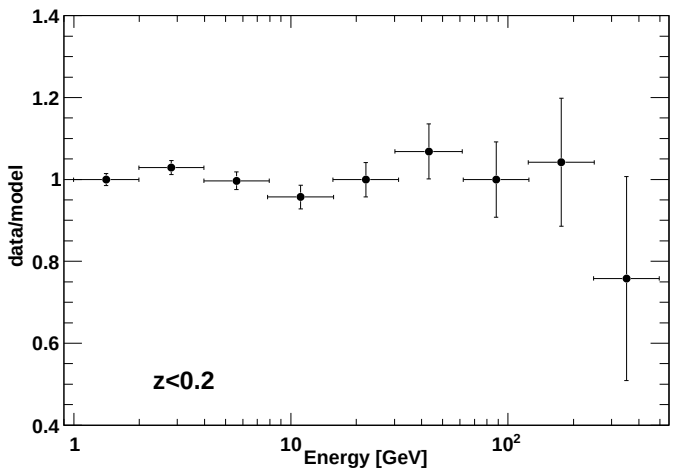

Figure S2 Average of the residuals with respect to the best fit models for all the blazars in the z<0.2 redshift bin.

the b parameter as reported in Table S1 represents the weighted average[5] of the 3 b values determined in the 3 redshift bins. For example, for the model of (*7*) we measure: b=1.18$^{+0.94}_{-0.81}$ (TS≈4 for z<0.2), b=0.82$^{+0.41}_{-0.30}$ (TS≈7 for 0.2≤z<0.5), and b=1.29$^{+0.43}_{-0.36}$ (TS≈25 for 0.5≤z<1.6). The weighted average yields (as reported in Table S1) $b = 1.02 \pm 0.23$ and TS≈36.

We also quantify the level of compatibility of the prediction of a given model with the *Fermi* data, by comparing the likelihood of the original model ($b = 1$) to the one of the best fit scenario (b free to vary). For b values significantly different than 1 a given EBL model predicts an attenuation larger than observed. Table S1 shows that the intensity of the optical-UV background in 4 of the 15 models we tested is not compatible with the *Fermi* data at $\geq 3\,\sigma$.

Figure S3 shows that the significance of the absorption feature is detected collectively[6] among the BL Lacs considered and is not attributable to just a few sources. Indeed, it is apparent that the TS increases linearly with the number of sources as expected in a background-limited scenario.

As shown already in Figure 1, our analysis probes absorption signatures that are a factor ∼4 times weaker than those probed in (*13*) which relied on only one year of data. Even a conservative 95 % upper limit derived from this analysis ($b_{UL} = 1.5$ referred to the model of (*7*), i.e. $\tau_{\gamma\gamma}$<0.6 at z≈1 and E=77 GeV) is a factor ∼2 below the one reported by (*13*).

Our analysis relies on the assumption that BL Lac spectra (and HSP in particular) do not change dramatically across the z=0.2 redshift barrier. In the next section we address possible sources of systematic effects.

[5]The weights are $1/\sigma_b^2$ where σ_b is the uncertainty on the b parameters.

[6]In Figure S3 the sources have been sorted in redshift from low to high redshift.

Table S1. Joint-likelihood results for different EBL models.

Model[a]	Ref.[b]	Significance of b=0 Rejection[c]	b[d]	Significance of b=1 Rejection[e]
Stecker et al. (2006) – fast evolution	(*23*)	4.6	0.10 ± 0.02	17.1
Stecker et al. (2006) – baseline	(*23*)	4.6	0.12 ± 0.03	15.1
Kneiske et al. (2004) – high UV	(*22*)	5.1	0.37 ± 0.08	5.9
Kneiske et al. (2004) – best fit	(*22*)	5.8	0.53 ± 0.12	3.2
Gilmore et al. (2012) – fiducial	(*27*)	5.6	0.67 ± 0.14	1.9
Primack et al. (2005)	(*56*)	5.5	0.77 ± 0.15	1.2
Dominguez et al. (2011)	(*25*)	5.9	1.02 ± 0.23	1.1
Finke et al. (2010) – model C	(*24*)	5.8	0.86 ± 0.23	1.0
Franceschini et al. (2008)	(*7*)	5.9	1.02 ± 0.23	0.9
Gilmore et al. (2012) – fixed	(*27*)	5.8	1.02 ± 0.22	0.7
Kneiske & Dole (2010)	(*26*)	5.7	0.90 ± 0.19	0.6
Gilmore et al. (2009) – fiducial	(*2*)	5.8	0.99 ± 0.22	0.6

[a]Models tested are implemented in the *Fermi* Science Tools. As an example the recent model of (*49*) which is not defined for E$\geq 250/(1+z)$ GeV could not be used, but its predictions are for completeness reported in Figure 1.

[b]Reference number in the 'References and Notes' section of the main text.

[c]Significance, in units of σ, of the attenuation in the spectra of blazars when a given EBL model is scaled by the factor b. In this case b=0 (i.e. no EBL absorption) constitutes the null hypothesis.

[d]This column lists the maximum likelihood values and 1 σ confidence ranges for the opacity scaling factor.

[e]Here the b=1 case (i.e. EBL absorption as predicted by a given EBL model) constitutes the null hypothesis. This column shows the compatibility (expressed in units of σ) of the predictions of EBL models with the *Fermi* observations. Large values mean less likely to be compatible.

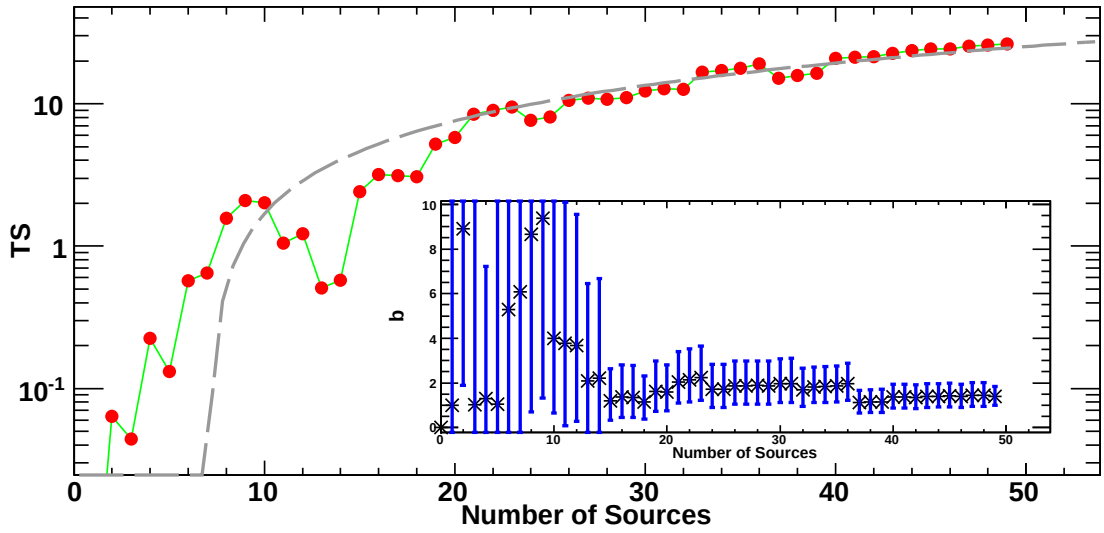

Figure S3 Increase in the TS value of the (renormalized) EBL model of (*7*) produced in the joint-likelihood fit (to the $0.5 \leq z < 1.6$ interval) while adding one source at a time. The sources have been sorted in redshift (from lowest to highest). The dashed line shows the best-fit linear increase of the TS with the number of sources. The inset shows the best-fit value of the renormalization parameter b applied to the opacity predicted by (*7*) (see text for details).

Validation of the Analysis using Simulations

We validated our analysis using simulated datasets starting from physically motivated spectral energy distributions (SEDs) of BL Lacs. We rely on SEDs that reproduce well the range of peak curvatures, peak frequencies (for both the synchrotron and high-energy component), and gamma-ray photon indices observed for the LAT-detected BL Lacs. These SEDs have been produced using the same numerical code presented in (*57*) and take into account all the important effects that contribute to determine the intrinsic curvature of the gamma-ray spectrum of the *Fermi* blazars. Of particular importance are those effects that depend on the curvature of the electron distribution, as well as those related to the Thomson (TH) to Klein-Nishina (KN) transition, in the inverse Compton process (IC). The latter effect is crucial since it is well known (*57, 58*) that the TH/KN transition in the IC cross section can result in a steepening of the high-energy branch of the IC SED, compared to the low-energy one. Our simulations fully take into account this effect, allowing us to study the potential bias in the EBL estimate.

We performed $\sim$500 simulations randomly selecting 50 SEDs from our template library. To each SED we assign a redshift (in the $0.5 \leq z < 1.6$ range) and a 0.1–100 GeV flux randomly extracted from those of BL Lacs in the second LAT AGN Catalog (*16*). We then proceeded to simulate the data expected from those sources based on *Fermi*'s instrument response function

and pointing history. Each one of those realizations was processed with the same analysis chain used on actual data.

Figure S4 presents the distribution of TS (left panel) and best-fit b parameters (right panel) for the simulated blazar population under the following two scenarios. First, no EBL attenuation was included, in order to check whether our analysis would pick a signal consistent with EBL attenuation when this was not present (i.e. a false positive). The dashed lines in the panels show that our analysis yields very small TS values and b values compatible with zero, as expected for a robust analysis.

In the second scenario, the SED models were attenuated using the opacities of the model of (*7*). The results summarized in Figure S4 show that TS values $\geq$20 and b values compatible with 1 (within the statistical uncertainty) are correctly retrieved. Moreover, the simulations show that our analysis is free of any major systematic uncertainty since the average values of b retrieved for both scenarios are compatible with the expected ones (0 and 1 respectively) within 1 %.

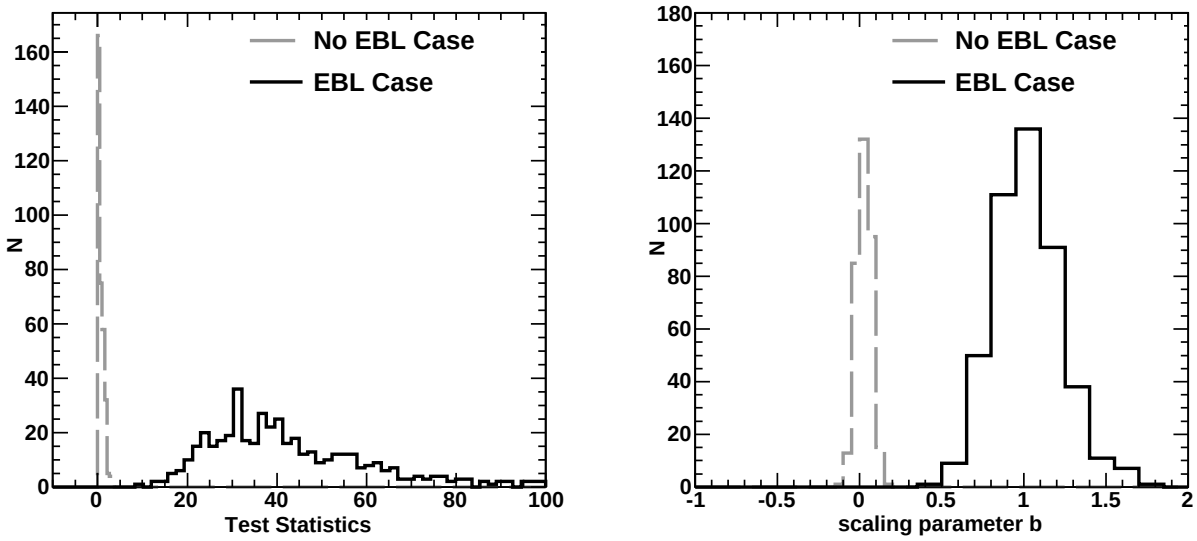

Figure S4 Results from joint-likelihood fits to the simulated datasets. The left panel shows the TS of the detection of the attenuation produced by the EBL for the case in which no EBL was applied to the SEDs (dashed line) and the case for which an attenuation consistent with the one of (*7*) was used (solid line). The right panel shows the best-fit b parameter for the same two scenarios.

Additional Tests

A number of additional tests have been performed to test the stability of the results presented in the previous sections. These are documented below.

Sample Selection

The selection criteria used in the previous sections were chosen *a priori* to yield a uniform source population that could be used to probe in a sensitive and least-biased way the EBL-induced absorption feature. Several tests have been performed to check this assumption.

The BL Lac population is known to evolve in redshift with HSP objects detected predominantly at low redshift and LSPs detected predominantly at larger redshifts with ISPs bridging the gap[7]. This could artificially induce a decline in the combined (produced by all subtypes) BL Lac spectrum at an energy that decreases with increasing redshift, and hence could mimic the effect of EBL-caused absorption. To test whether such bias affects our results we run the analysis separately for the three source classes (HSPs, ISPs and LSPs). For each of them we define two redshift bins: z$<$0.2 and z$\geq$0.2. In the lowest redshift bin, due to the low statistics[8] the joint likelihood yields no significant detection of EBL softening. For the HSPs in the low redshift bin, the joint likelihood yields b=1.46$^{+0.89}_{-0.78}$ and a TS=4.1. At higher redshift, the results are: b =1.04$^{+0.32}_{-0.28}$ (TS=24), b =2.13$^{+1.11}_{-0.98}$ (TS=9), and b =0.43$^{+0.67}_{-0.71}$ (TS=1), for HSPs, ISPs and LSPs respectively. The weighted average of the above values yields b =1.04$^{+0.27}_{-0.24}$ and a total TS of $\sim$38. These results are in very good agreement with the ones presented in the previous sections and show that high-redshift LSPs are not responsible for the observed spectral softening, and HSPs are mainly responsible for it. Moreover, since the signal is dominated by only one source population (namely HSPs) the probability that selection effects from changing the sample composition with redshift strongly affect our result is rather low.

We also checked if the highest redshift HSPs are driving the result. To this extent we isolated (from the above sample) the 6 HSPs with the highest redshift. The joint likelihood yields a TS=6 and b =1.99$^{+1.83}_{-1.10}$ indicating that the detection of the EBL cut-off is not caused by a few high redshift sources.

We also tested the population of BL Lacs that did not pass our selection criteria. This comprises 32 objects detected with a rather low significance in the 3-10 GeV over a redshift range 0.03-1.9 (average of 0.4). The joint likelihood yields b=1.93$^{+2.73}_{-1.39}$ and TS=3.5 compatible with our result. Thus, including low significance sources marginally improves the results of our analysis.

[7] The sample used in the previous sections contains for z$<$0.2 35 HSPs, 10 ISPs and 5 LSPs. The 0.2$\leq$z$<$0.5 sample comprises 27 HSPs, 18 ISPs, 5 LSPs, while the z$\geq$0.5 sample contains 10 HSPs, 19 ISPs, and 21 LSPs.

[8] In the z$<$0.2 bin there are respectively 41 HSPs, 10 ISPs and 5 LSPs; while in the z$\geq$0.2 there are 50 HSPs, 30 ISPs, and 23 LSPs.

Binning in Redshift

We bin the sources in redshift to cope with the maximum number of free parameters (i.e. 100) that can be optimized in a single maximum likelihood fit. Our analysis is however independent of the redshift binning used. This is already evident from the tests reported above using separately HSPs, ISPs and LSPs and a different redshift binning (with respect to the one used in the main analysis). However, we performed an additional test and divided the most constraining redshift bin (i.e. $0.5 \leq z < 1.6$) into halves (at $z \approx 0.75$) containing 25 sources each. When fitting the *Fermi* data using the model of (*7*), we obtain b=$1.71^{+1.12}_{-0.82}$ (TS=10) and b=$1.17^{+0.47}_{-0.39}$ (TS=15.4) for the $0.5 \leq z < 0.75$ and $0.75 \leq z < 1.6$ bins respectively. The weighted average of the above values yields b=$1.26^{+0.43}_{-0.35}$ and the total TS=25.4. This can be compared to b=$1.29^{+0.43}_{-0.36}$ and TS=25.1 obtained for the full $0.5 \leq z < 1.6$ redshift bin. Our analysis is thus robust against choices of the redshift bins.

Source Variability

Blazars are inherently variable objects with variability in flux of up to a factor 10 or more. Throughout this work we use spectra of blazars accumulated over 46 months of observations and blazar variability might in principle bias our result. In the *Fermi* sample, the most variable BL Lac objects are those belonging to the LSP and ISP class and it has been shown already that the entire analysis can be confirmed without using those two classes.

To test possible biases deriving from variability we selected the 30 most variable, according to (*16, 21*), and most significant (in the 3–10 GeV band) BL Lac objects. Repeating the entire analysis using this sample, we obtain $b = 1.20^{+0.62}_{-0.52}$ and a TS=9. These results are in good agreement with the ones presented in the previous section and show that blazar variability does not affect our results.

Critical Energy

Our measurement relies on the extrapolation of the intrinsic (i.e. unabsorbed) spectrum above the critical energy E_{crit}. Aggressive choices of this energy (i.e. large values) might bias the result towards a low level of opacity. We show that this is not the case for our measurement and that our analysis is robust against conservative choices of E_{crit}. In order to demonstrate it, we imposed E_{crit}=10 GeV for any source in the most constraining redshift interval: i.e. $0.5 \leq z < 1.6$. For most EBL models, with the exception of those presented in (*23*), the opacity is negligible at 10 GeV up to $z \approx 1.6$. When fitting the *Fermi* data using the model of (*7*), our analysis yields a value of b=$1.24^{+0.44}_{-0.37}$ and TS≈22 for the constant E_{crit}=10 GeV case. This can be compared to b=$1.29^{+0.43}_{-0.36}$ and TS≈25.1 for the variable E_{crit} case presented in the main text. We thus conclude that our analysis is robust against any conservative choice of E_{crit}.

Systematic Uncertainties of the Instrument Response Function

In order to gauge the systematic uncertainties of this analysis we use the IRF bracketing method as described in (*59*). By deriving two different sets of IRFs and repeating the entire analysis we find that the systematic uncertainty on the opacity $\tau_{\gamma\gamma}$ is of the order $\sim$7 %.

Moreover, the entire analysis has been repeated using the P7CLEAN_V6 photon selection and IRF. The results presented in the above sections are fully confirmed and the systematic uncertainty on the opacity $\tau_{\gamma\gamma}$ due to changing event selection and IRF is of the order 3 %. Thus, we consider the total systematic uncertainty on $\tau_{\gamma\gamma}$ to be $\sim$10 %.

Source Intrinsic Effects

The blazar evolution with luminosity as described by the blazar sequence (*31–34*) and the change of blazar type with redshift might in principle produce an intrinsic cut-off that changes with redshift. An intrinsic spectral cut-off might be detected if the part of the blazar spectrum sampled by *Fermi* corresponds to the tail of the electron distribution. In our case, this might happen only for the LSP sources and it has already been shown (see previous section) that their contribution to the total signal is negligible. On the other hand most of the signal is dominated by HSPs that are detected by *Fermi* right below or at the peak of the inverse Compton component, thus excluding the possibility that their emission is produced in the tail of the electron distribution.

However, in order to study the compatibility of the detected signal with an intrinsic origin, we assumed that all blazars have an exponential cut-off at a source-frame energy E_0. We also assumed that the blazar spectrum moves to lower frequency for increasing source luminosity as dictated by the so-called blazar sequence (*31–34*). This might represent the case in which the maximum electron energy depends on the jet power or the luminosity. Figure 2 shows that this model (E_0 is fitted to the data) provides a poor representation of the *Fermi* data. Even assuming that the maximum electron energy depends on a variable power of the luminosity does not improve the results. The result is even worse if the blazar sequence is not invoked. We thus conclude that the impact of source intrinsic effects on our analysis is likely minor.

Reprocessed Emission

The electron-positron pairs generated in the interaction of gamma rays and EBL photons can initiate a cascade by subsequent Compton scattering of the photons of the Cosmic Microwave Background. Typically the cascades originated by TeV gamma rays are reprocessed in the GeV energy range. In the case of a weak intergalactic magnetic field (IGMF), the pairs are not deflected out of the line of sight (*60*) and the reprocessed emission can be a substantial fraction of (or even dominate) the total source signal in the $\lesssim$100 GeV band. The intensity of the reprocessed emission depends primarily on the EBL density, on the intensity of the IGMF, on its coherent length and on the position of the peak of the high-energy component of a blazar (*61*). For typical coherent lengths of $\sim$1 Mpc and SED peaks located at or below 10 TeV, lower limits

of B$\gtrsim 10^{-15}$ G have been inferred (*61, 62*). For these intensities of the IGMF the reprocessed emission is expected to be subdominant with respect to the intrinsic component (*63*). While it is true that these estimates are based on an implied activity of the source of a few million years (*64*), the majority of the *Fermi* BL Lacs is expected to have the peak of the high-energy component located at $\leq$1 TeV (*65*) greatly reducing the amount of reprocessed emission in the GeV band (*61*). Similar considerations (i.e. suppression of the reprocessed emission by the IGMF) hold also for the case in which blazars are also sources of ultrahigh energy cosmic rays (*66–68*).